2024 European Control Conference (ECC)
June 25-28, 2024. Stockholm, Sweden

Health-Conscious Model Predictive Control for Integrated Shipboard Power Systems with Generator and Battery Under High Ramp Rate Loads

Mitchell Levi[1], Satish Vedula[2], Olugbenga Moses Anubi[2], Heath Hofmann[3], and Jing Sun[1]

Abstract— **Energy storage on all-electric vessels can enable shipboard-integrated power systems to meet increasing pulse load requirements and reduce fuel consumption and greenhouse gas emissions. However, integrating energy storage into shipboard power systems imposes additional requirements on the power management systems. In this paper, a power management controller is developed for the integrated power system utilizing a model predictive control (MPC) scheme. The MPC formulations developed here aim to manage the competing requirements of minimizing component health degradation and the power tracking error when responding to high ramp rate power demands. Sensitivity analysis is performed to explore the direct trade-off between generator health and battery health when meeting the load power demand is strictly enforced. The MPC solution is demonstrated for varying energy storage sizes to provide insight for the design and operation of an integrated shipboard power system.**

I. INTRODUCTION

Increasing regulations on greenhouse gas emissions in the maritime shipping industry has driven ship electrification. As the installed electric load increases, more energy storage systems have been incorporated to improve energy efficiency, enhance power quality, and ensure reliability [1]. In [2], the hybrid propulsion architectures studied are shown to reduce emissions and fuel consumption by 10-35%.

To take advantage of the different characteristics of the energy sources and maximize the fuel-saving potential of these hybrid power systems, advanced energy management systems (EMS) are needed. Among many functions performed by the EMS, meeting load power demands while enforcing the physical constraints of the propulsion plant is essential [3]. Lifecycle and health protection of power systems are important attributes in EMS design. Although generator ramp-rate limits can be increased in response to pulsed power loads, this decreases the lifetime of the generators due to increased wear and tear and could even trigger sudden failure. Meanwhile, over-cycling or high depth of discharge can cause performance degradation in energy storage units [4]. The energy management strategy must minimize power-tracking errors while also mitigating the impact on the system's health.

Predictive control has been extensively studied for shipboard energy management systems. In [5], a predictive energy management strategy is proposed on an autonomous ship with batteries. The authors use the predicted trajectory to estimate future required power. The optimal energy split between generators and batteries is then solved using the formulated power prediction. In [6], an equivalent strategy is used with MPC to minimize fuel consumption. The power split between the diesel generator, battery, and ultra-capacitor energy storage is determined by assigning an equivalent factor to the battery and ultra-capacitor to convert their electrical powers into an equivalent fuel consumption. An MPC framework is proposed in [7] that aims to minimize fuel consumption on a vessel with four diesel generators, batteries, two main engines, and shaft generators for power take-off/power take-in. Fuel savings are shown for multiple operating profiles.

Additionally, predictive control strategies have been proposed for specifically meeting the pulse load demands on a shipboard power system. In [1], [8], and [9] predictive control algorithms to coordinate the generator and energy storage are utilized to meet the propulsion power demand and a pulsed power load while enforcing generator and energy storage rate limits. In [10], an adaptive MPC formulation is proposed to handle parameter uncertainty and fluctuating power demand on a vessel with batteries and ultra-capacitors. MPC with load prediction is demonstrated in [11] for shipboard power and energy management, where the authors show that the system component constraints can be met and a specific final state of charge (SoC) can be enforced. In [12] and [13], real-time MPC-based power management is demonstrated with an IPA-SQP approach and Interior Point Optimizer, respectively. These papers show the power management controller results on a real-time simulator and a physical test bed representing two generators under square-wave pulse loads. In these approaches, component wear is reduced by penalizing the generator power ramp rate. The authors show the sensitivity between the ramp rate penalty and the tracking error performance.

Contribution: While the approaches in [1, 8, 9, 14, 10, 11] take into account the dynamic constraints of the generators and/or energy storage systems, they do not discuss the trade-off between component health and tracking performance. In [12, 13], the generator ramp rate limits are

[1]Mitchell Levi and Jing Sun are with the Department of Naval Architecture and Marine Engineering, University of Michigan, Ann Arbor, MI 48109 USA

[2]Satish Vedula and Olugbenga Moses Anubi are with the Department of Electrical and Computer Engineering, Center for Advanced Power systems, Florida State University, Tallahassee, FL 32310, USA

[3]Heath Hofmann is with the Department of Electrical Engineering and Computer Science, University of Michigan, Ann Arbor, Michigan 48109, USA

adjusted and tracking performance is evaluated. However, the integration of energy storage is not explored. In this paper, we develop an MPC formulation for power tracking of an integrated power system with generator sets and batteries. Through case studies, we quantify the trade-off between generator and battery health protection when tracking a high-ramp-rate load profile.

This paper is organized as follows: Section II introduces the readers to the notations used throughout the paper and the shipboard power system model. This section also describes the design of the power profile. A proposed power tracking and battery health MPC control algorithm and simulation results are presented in Section III. In Section IV, sensitivity analysis is introduced to evaluate the component health trade-off. Finally, Section V concludes the paper.

II. SYSTEM MODEL

In this section, we give the mathematical notations used throughout the paper followed by the shipboard power system (SPS) model and the hierarchical control structure for the SPS. Then, we present the mathematical modeling of the components in the SPS. The space of natural numbers is represented by $\mathbb{N}$, and the space of real numbers is denoted by $\mathbb{R}$. $\mathbb{R}_+$ denotes a positive real number. The space of real vectors of n elements is denoted by $\mathbb{R}^n$, real matrices consisting of n rows and m columns are denoted as $\mathbb{R}^{n\times m}$. Natural and real scalars are both denoted by lower-case letters (i.e. $u \in \mathbb{N}$ and $u \in \mathbb{R}$). Real vectors are represented by lower-case bold letters (i.e. $\mathbf{s} \in \mathbb{R}^n$). The vector consisting of all ones is denoted as $\mathbf{1}_m \in \mathbb{R}^m$.

A. Notional 4-Zone Shipboard Power System

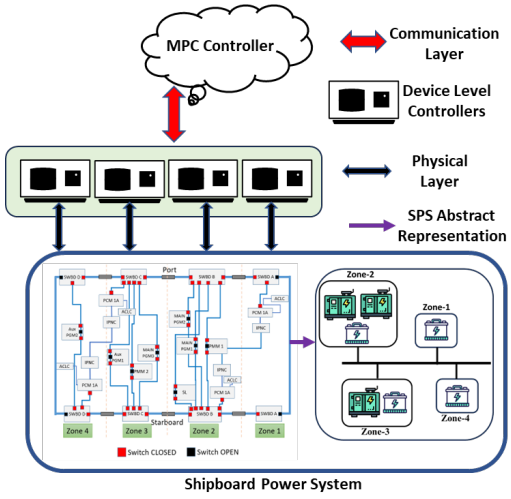

Fig. 1. Notional 4-Zone SPS Model and its hierarchical control structure

Figure 1 depicts the zonal representation of SPS and the hierarchical control structure for SPS. The control structure was designed as a two-level control scheme consisting of an upper-level energy management MPC layer and a lower device-level control layer (DLC) [15]. More insight into the DLC is provided in the next subsection. The upper/MPC layer acts as a reference power generator for the lower device level controller. All 4 zones are unified through a common $12kV$ DC bus. The common bus voltage is regulated utilizing a DLC. Each zone consists of: numerous power-supplying sources such as power generation modules (PGMs), which contain fuel-operated generators, power conversion modules (PCMs), which consist of numerous battery modules lumped together, and power-consuming loads such as propulsion motor modules (PMMs). In this work, only the key elements in the SPS model were considered such as the PGMs, PCMs (batteries), and PMMs. The power demand and supply must be balanced within some acceptable tolerance. Thus, the power flow in the SPS is given as follows:

$$\sum_{i=1}^{n} p_{g_i}(t) + \sum_{j=1}^{m} p_{b_j}(t) - p_d(t) = 0, \tag{1}$$

where $p_{g_i}, p_{b_j}, p_d \in \mathbb{R}$ are powers corresponding to the generator, battery energy storage element, and power demand respectively.

B. PGM, Battery and Power Load Modeling

The PGM model consists of a current-controlled DC voltage source coupled with a series RL impedance connected to the bus, whose voltage was assumed to be regulated to a set point. A dynamical model consisting of n PGMs is given as follows:

$$l_g \frac{d\mathbf{i}_g}{dt} = -r_g \mathbf{i}_g + v_{bus}\mathbf{1}_n - \mathbf{v}_g, \tag{2}$$

where $\mathbf{i}_g \in \mathbb{R}^n$ are the generator currents, and $\mathbf{v}_g \in \mathbb{R}^n$ are the controllable voltage sources. The generator inductance l_g is in Henrys, r_g is the generator resistance in Ohms, and v_{bus} is the bus voltage to which the PGMs are coupled. As mentioned, the assumption was that the bus voltage is being regulated to a set point and is already at steady state. The current injected by the PGMs into the bus is dictated by controlling this voltage source. Given an optimal power profile $\mathbf{p}_{g_r}$ from the upper layer control, the reference current $\mathbf{i}_{g_r} \in \mathbb{R}^n$ is generated as: $\mathbf{i}_{g_r} = \mathbf{p}_{g_r}/v_{bus}$ and the local DLC input $\mathbf{v}_g$ is determined via a closed loop control scheme in which the device level states track the reference current such that

$$\left\|\tilde{\mathbf{i}}_g(t)\right\| \leqslant \left\|\tilde{\mathbf{i}}_g(t_0)\right\| e^{-\lambda(t-t_0)}, \forall\ t \geqslant t_0 \geqslant 0 \tag{3}$$

where $\tilde{\mathbf{i}}_g = \mathbf{i}_g - \mathbf{i}_{g_r}$ is the tracking error associated with the PGM currents and $\lambda > 0$. We assumed that there exists a continuously differentiable, positive definite function $V : \mathbb{R}^n \to \mathbb{R}$ satisfying [16]

$$k_1(\|\tilde{\mathbf{i}}_g\|) \leqslant V \leqslant k_2(\|\tilde{\mathbf{i}}_g\|), \quad \frac{\partial V}{\partial \tilde{\mathbf{i}}_g}\dot{\tilde{\mathbf{i}}}_g \leqslant -k_3(\|\tilde{\mathbf{i}}_g\|).$$

Thus, there exists a stabilizing controller of form $\mathbf{v}_g = k(\tilde{\mathbf{i}}_g)$ [16]. We assumed that the device-level controller dynamics are significantly faster than the high-level controller.

The battery model consists of multiple energy storage systems (ESSs) which were modeled as a current-controlled

voltage source and a resistance r_b coupled to the bus. The battery current i_b is dictated by the controllable voltage source v_b. The open circuit voltage v_{oc} is a function of the battery state of charge (SoC). The relation between v_{oc} and SoC can be approximated using various functions ranging from lower to higher orders with the linear approximation being the fundamental one given as $v_{oc} = c_1 SoC + c_2$, where c_1, c_2 are constants [17]. Since the battery voltage dynamics are fast compared to SoC dynamics, they are neglected and the control input $\mathbf{v}_b \in \mathbb{R}^m$ is determined through

$$\mathbf{v}_b = \mathbf{v}_{bus} - \frac{\mathbf{p}_{b_r}\mathbf{r}_b - \mathbf{v}_{bus}\mathbf{v}_{oc}}{\mathbf{v}_{bus}},$$
$$\mathbf{i}_b = \frac{\mathbf{v}_{bus} - \mathbf{v}_b - \mathbf{v}_{oc}}{\mathbf{r}_b},$$

where $\mathbf{p}_{b_r}$ is the optimal power profile from the upper-level controller.

The discretized dynamic model for the SoC is given for the m number of batteries as follows:

$$\mathbf{SoC}_{k+1} = \mathbf{SoC}_k - T_s \frac{\mathbf{i}_b}{Q}, \tag{4}$$

where T_s is the discretization time-step, $\mathbf{i}_b \in \mathbb{R}^m$ denotes the battery current vector, $\mathbf{SoC} \in \mathbb{R}^m$ the SoC vector, and Q the total capacity of an individual battery pack in $ampere-hours$. We assume that all battery modules have the same capacity; however, the technique can be easily generalized to handle different capacities.

The power load was modeled as a resistive load whose current can be controlled by means of a controllable voltage v_L based on the power demand. Given a power demand p_L, the controllable load voltage v_L, which determines the load current i_L is given as:

$$v_L = v_{bus} - \frac{p_L r_L}{v_{bus}},$$
$$i_L = \frac{v_{bus} - v_L}{r_L},$$

where r_L is the load resistance. The assumption made in designing the load was that there is only one load module that consumes the power generated by n PGMs and m batteries. Thus $p_L, v_L \in \mathbb{R}$.

Onboard the vessel being studied there are three generators with a total installed generator power of 29 megawatts. The baseline number of modules used is 15 with a capacity of 20 amp-hours each. In the next section, we present the high-level control designed using an MPC scheme. The model and the nominal device-level control design developed in this section act as a base for the deployment of the high-level controller.

III. POWER TRACKING AND BATTERY HEALTH

In this section, the controller formulation was developed to minimize the power tracking error and the battery health degradation over the power demand profile. Within the developed MPC formulation, the generator ramp rate was held constant so that battery health and the tracking performance could be compared directly. Using this controller the sensitivity to the prediction horizon was tested in MATLAB-SIMULINK. A fixed-step simulation time of $10^{-3} sec$ was used for simulation. The MPC updates the control at a slower rate of $1 sec$. The performance of the proposed power management controllers are tested against the power demand profile shown in Figure 2, which includes both pulse-power loads and other high-ramp-rate loads.

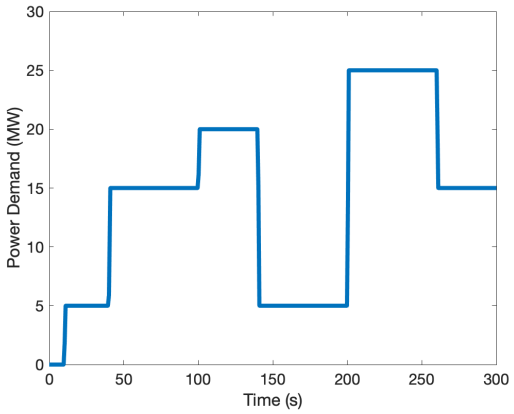

Fig. 2. Load Profile Tested in Simulations

In the formulation presented below, the cost function includes the square of the tracking error and the battery usage cost.

Minimize:

$$\begin{aligned}
&\sum_{j=k}^{k+h-1} (p_{f_j} - p_{g_j} - p_{b_j})^2 + \alpha * log\left(\frac{\frac{-|i_{b_j}|}{Q}+\beta}{\beta}\right),\\
&\text{s.t.} \quad p_g^{min} \preceq p_{g_j} \preceq p_g^{max},\\
&\qquad R_{g_j} = p_{g_j} - p_{g_{j-1}},\\
&\qquad -R_g \preceq R_{g_j} \preceq R_g,\\
&\qquad p_{b_j} = (v_{oc} i_{b_j} - i_{b_j}^2 r_b) m,\\
&\qquad SoC_{j+1} = SoC_j - \frac{i_{b_j}}{Q},\\
&\qquad SoC^{min} \preceq SoC_j \preceq SoC^{max},
\end{aligned} \tag{5}$$

where $p_{f_j}, p_{g_j}, p_{b_j} \in \mathbb{R}$ denotes the forecasted power, the power injected by the PGM, and the power injected by the batteries at every instant in the horizon. The battery current per module is denoted by $i_{b_j} \in \mathbb{R}$. The lower and upper power limitations on the PGMs are p_g^{min} and p_g^{max} respectively. The ramp-rate of the generator is R_{g_j} at every instant in the horizon, and R_g is the limit on the ramp-rate magnitude. The lower and upper SoC limitations are denoted SoC^{min} and SoC^{max}, respectively. PGM and Battery powers are used in initializing the optimization problem in (5).

Battery usage was penalized using a logarithmic barrier function. The tunable barrier function was chosen to capture an upper limit of the battery module current with the $\beta \in \mathbb{R}_+$ parameter, while the battery usage cost was adjusted with the $\alpha \in \mathbb{R}_+$ weighting parameter. Figure 3 shows the battery

usage cost for different β values used in the logarithmic barrier function. Unless otherwise noted, the results shown in this paper use a set of baseline parameters. The MPC controller uses a prediction horizon of 10 seconds and $\beta = 10$.

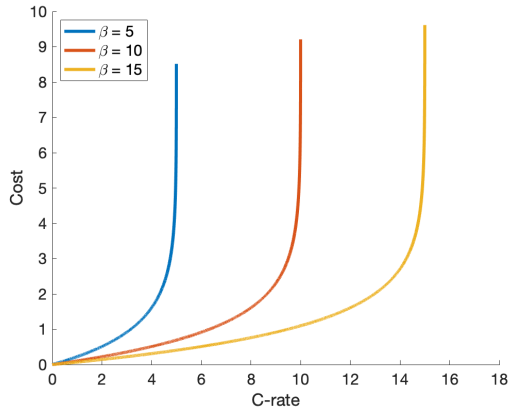

Fig. 3. Battery Usage Cost (W^2) with Different β Values

In the first set of simulations the generator ramp rate limit was a fixed constraint in the MPC formulation. With the ramp rate of the generator constrained, root mean square (RMS) power tracking error is compared to the RMS C-rate of the battery modules to represent the state of health degradation of the battery over the load profile. This metric is used because a higher battery C-rate has been shown to lead to capacity loss and decrease the cycle life of the battery [18]. The RMS power tracking error and RMS C-rate is calculated by the following equation defining the RMS of a variable x:

$$RMS = \sqrt{\frac{1}{N}\sum_{j=1}^{N} x_j{}^2}, \tag{6}$$

where N is the number of data points and x_j is the evaluated variable.

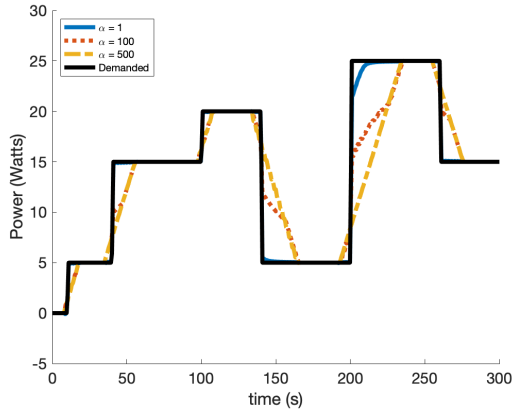

Fig. 4. Power Tracking Performance with Different Battery Usage Weighting

The power tracking performance of the power management controller for three different battery usage weightings is shown in Figure 4. The yellow dashed line represents a large battery usage weighting, where the battery is not used, and hence represents the best possible power tracking performance when using only generators. The solid blue line shows the performance where the battery is used heavily, and the dotted red line is a case in between those two. When the battery usage weighting is equal to one, the power demand and power generated nearly overlap.

In Figure 5, the RMS power tracking error and RMS C-rate of the battery over the load profile is shown as a function of the battery usage weighting. The relationship shows the expected tradeoff between battery usage and power tracking performance.

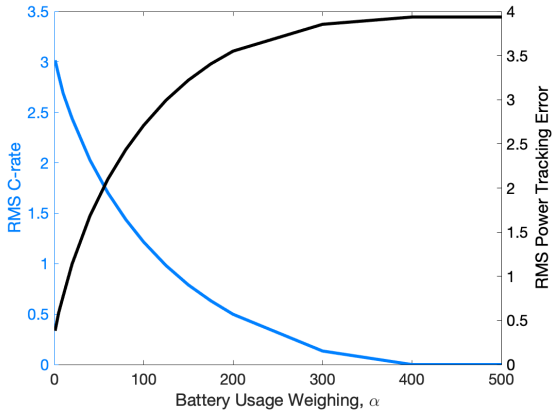

Fig. 5. RMS Power Tracking Error and RMS Battery C-rate for Different Battery Usage Weighting

The prediction horizon h is a design variable in MPC. To select its value, the sensitivity to the prediction horizon of the MPC controller was explored. The performance of the responses for MPC with a prediction horizon length of 2s to 30s was evaluated. The simulations were run with a constant value for the battery usage weighting α. The results show the improved performance with a longer controller prediction horizon. Diminishing returns in both RMS power tracking error and RMS C-rate can be observed. The computation time for four different prediction horizon lengths is quantified in Table I. Based on the sensitivity analysis, a prediction horizon of $h = 10$ was selected. With the results from this MPC formulation, it can be seen that there is a clear tradeoff between battery state of health and the power tracking of the SPS.

IV. BATTERY AND GENERATOR HEALTH TRADE-OFF

In this section, an MPC formulation was developed to evaluate the cost of generator and battery usage. This was done under the constraint that the power demand is to be fully met by the battery and generators. With this requirement, high-ramp-rate loads will impact the battery and generator health. The predictive control allows the EMS to manage

TABLE I

COMPUTATION TIME FOR DIFFERENT PREDICTION HORIZON LENGTHS

Prediction Horizon (s)	Computation Time (s)	RMS C-rate	RMS Power Tracking Error (MW)
2	0.3058	3.6207	1.1625
10	0.6077	2.8662	0.5884
20	1.3467	2.6473	0.4341
30	2.7323	2.6393	0.4261

the degradation and make the proper trade-off. Once again the battery state of health degradation was represented by the RMS C-rate. The generator state of health degradation is impacted by the RMS generator ramp rate, as shown in [8, 12]. Therefore, it is used in the cost function of the MPC optimization. To evaluate the trade-off between generator health and battery health, the MPC formulation shown below was explored through simulations.

$$\begin{aligned}
\text{Minimize:} \quad & \sum_{j=k}^{k+h-1} \left(R_{g_j}\right)^2 - \alpha * log\left(\frac{\frac{-|i_{b_j}|}{Q} + \beta}{\beta}\right) \\
\text{s.t.} \quad & p_{f_j} = p_{g_j} + p_{b_j}, \\
& p_g^{min} \preceq p_{g_j} \preceq p_g^{max}, \\
& R_{g_j} = p_{g_j} - p_{g_{j-1}}, \\
& -R_g \preceq R_{g_j} \preceq R_g, \\
& p_{b_j} = (v_{oc} i_{b_j} - i_{b_j}^2 r_b) m, \\
& SoC_{j+1} = SoC_j - \frac{i_{b_j}}{Q}, \\
& SoC^{min} \preceq SoC_j \preceq SoC^{max}.
\end{aligned} \tag{7}$$

In this formulation, the load power demand is imposed as a hard constraint. The objective function includes terms associated with the generator ramp rate and the battery C-rate. Minimizing the objective function represents the effort to protect the health of the components. All of the parametric notations described in Section-III for equation (5) are the same as the MPC problem in (7). The power profile shown in Figure 2 was used again to simulate a series of high-ramp-rate events.

The results from simulations with 15 battery modules are shown in Figure 6, where the usage of the battery and generator can be seen for different α weightings. In Figure 7 the RMS C-rate of the battery and the RMS generator ramp rate are plotted as a function of battery usage weighting.

Finally, the trade-offs between generator health and battery health were explored for different energy storage sizes. In Figure 8 the relationship between generator ramp rate and battery C-rate is shown for varying sizes of energy storage. The impact of adding more battery modules onboard is shown to decrease the average C-rate down and/or decrease the average generator ramp rate.

V. CONCLUSIONS

In this paper, two trade-offs were explored using model predictive control (MPC) for a power management system. The trade-off between battery health and power tracking

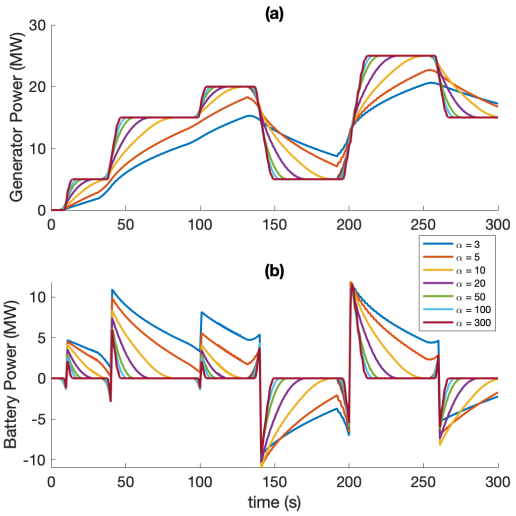

Fig. 6. Power Split Results with 15 Battery Modules. (a) Generator Power Demand. (b) Battery Power Demand

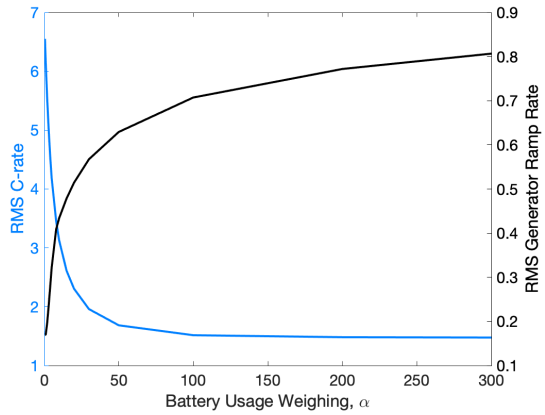

Fig. 7. Battery RMS C-rate and RMS Generator Ramp Rate vs Battery Usage Weighting with 15 Battery Modules

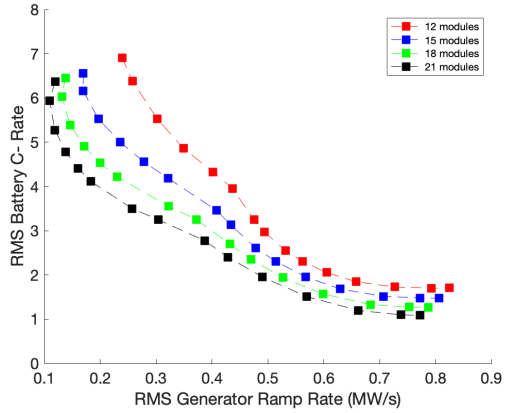

Fig. 8. Battery RMS C-rate versus RMS Generator Ramp Rate for Different Size Energy Storage

ability was evaluated as well as the trade-off between battery health and generator health. For the first comparison the MPC formulation held the maximum allowed generator ramp rate constant and the power tracking error and battery usage were minimized. In the second formulation the generator ramp rate and battery usage was minimized while enforcing a power tracking condition. In both MPC cost functions the battery usage cost was calculated using a logarithmic barrier function to represent physical component constraints and reduce the penalty on low C-rate usage.

The proposed MPC formulations provide tools to assist designers in designing a diesel electric ship with energy storage. For example, Figure 8 can be used for sizing the battery storage units. Different tuning parameters such as α for the weighting, β in the barrier function, and h for the prediction horizon can be properly chosen to reflect different priorities and to explore the design space.

While the proposed MPC formulation was demonstrated with one loading profile in this case study, the approach is generalizable with a wide range of possible ramp rates. A real operational power profile could further provide insights to energy storage sizing for any given vessel. For future study, the MPC formulations can be expanded to include the power tracking error and both the battery C-rate and generator ramp rate together. The cost of battery usage can also be modeled to directly capture battery degradation mechanisms. An asymmetrical barrier function that penalizes charge and discharge rates differently could be explored to more accurately capture the impact to battery state of health.

ACKNOWLEDGMENT

This work was sponsored by U.S Office of Naval Research grants N00014-18-1-2330 and N00014-22-1-2442.

REFERENCES

[1] T. V. Vu, D. Gonsoulin, F. Diaz, C. S. Edrington, and T. El-Mezyani, "Predictive control for energy management in ship power systems under high-power ramp rate loads," *IEEE Transactions on Energy Conversion*, vol. 32, no. 2, pp. 788–797, 2017.

[2] R. Geertsma, R. Negenborn, K. Visser, and J. Hopman, "Design and control of hybrid power and propulsion systems for smart ships: A review of developments," *Applied Energy*, vol. 194, pp. 30–54, 2017.

[3] N. Planakis, G. Papalambrou, and N. Kyrtatos, "Ship energy management system development and experimental evaluation utilizing marine loading cycles based on machine learning techniques," *Applied Energy*, vol. 307, p. 118 085, 2022.

[4] K. Hein, Y. Xu, G. Wilson, and A. K. Gupta, "Coordinated optimal voyage planning and energy management of all-electric ship with hybrid energy storage system," *IEEE Transactions on Power Systems*, vol. 36, no. 3, pp. 2355–2365, 2021.

[5] A. Haseltalab and R. R. Negenborn, "Model predictive maneuvering control and energy management for all-electric autonomous ships," *Applied Energy*, vol. 251, p. 113 308, 2019.

[6] P. Xie, S. Tan, J. M. Guerrero, and J. C. Vasquez, "Mpc-informed ecms based real-time power management strategy for hybrid electric ship," *Energy Reports*, vol. 7, pp. 126–133, 2021.

[7] S. Antonopoulos, K. Visser, M. Kalikatzarakis, and V. Reppa, "Mpc framework for the energy management of hybrid ships with an energy storage system," *Journal of Marine Science and Engineering*, vol. 9, p. 993, Sep. 2021.

[8] T. V. Vu, D. Gonsoulin, D. Perkins, F. Diaz, H. Vahedi, and C. S. Edrington, "Predictive energy management for mvdc all-electric ships," in *2017 IEEE Electric Ship Technologies Symposium (ESTS)*, 2017, pp. 327–331.

[9] D. Gonsoulin, T. Vu, F. Diaz, H. Vahedi, D. Perkins, and C. Edrington, "Centralized mpc for multiple energy storages in ship power systems," in *IECON 2017 - 43rd Annual Conference of the IEEE Industrial Electronics Society*, 2017, pp. 6777–6782.

[10] J. Hou, J. Sun, and H. Hofmann, "Adaptive model predictive control with propulsion load estimation and prediction for all-electric ship energy management," *Energy*, vol. 150, pp. 877–889, 2018.

[11] M. M. Bijaieh, S. Vedula, and O. M. Anubi, "Model and load predictive control for design and energy management of shipboard power systems," in *2021 IEEE Conference on Control Technology and Applications (CCTA)*, 2021, pp. 607–612.

[12] H. Park *et al.*, "Real-time model predictive control for shipboard power management using the ipa-sqp approach," *IEEE Transactions on Control Systems Technology*, vol. 23, no. 6, pp. 2129–2143, 2015.

[13] P. Stone *et al.*, "Shipboard power management using constrained nonlinear model predictive control," in *2015 IEEE Electric Ship Technologies Symposium (ESTS)*, 2015, pp. 1–7.

[14] J. Hou, Z. Song, H. Hofmann, and J. Sun, "Adaptive model predictive control for hybrid energy storage energy management in all-electric ship microgrids," *Energy Conversion and Management*, vol. 198, p. 111 929, Oct. 2019.

[15] T. ESRDC, "Model description document notional four zone mvdc shipboard power system model," *ESRDC Website, www.esrdc.com*, 2017.

[16] H. Khalil, *Nonlinear Systems* (Always Learning). Pearson, 2015.

[17] C. Weng, J. Sun, and H. Peng, "An open-circuit-voltage model of lithium-ion batteries for effective incremental capacity analysis," 2013.

[18] Z. Song, J. Li, J. Hou, H. Hofmann, M. Ouyang, and J. Du, "The battery-supercapacitor hybrid energy storage system in electric vehicle applications: A case study," *Energy*, vol. 154, pp. 433–441, 2018.